Spatial distribution and frequency of precipitation during an extreme event: July 2006 mesoscale convective complexes and floods in southeastern Arizona

Peter G. Griffiths,[1] Christopher S. Magirl,[2] Robert H. Webb,[1] Erik Pytlak,[3] Peter A. Troch,[4] and Steve W. Lyon[5]

Received 20 August 2008; revised 28 February 2009; accepted 11 May 2009; published 23 July 2009.

[1] An extreme, multiday rainfall event over southeastern Arizona during 27–31 July 2006 caused record flooding and a historically unprecedented number of slope failures and debris flows in the Santa Catalina Mountains north of Tucson. An unusual synoptic weather pattern induced repeated nocturnal mesoscale convective systems over southeastern Arizona for five continuous days, generating multiday rainfall totals up to 360 mm. Analysis of point rainfall and weather radar data yielded storm totals for the southern Santa Catalina Mountains at 754 grid cells approximately 1 km × 1 km in size. Precipitation intensity for the 31 July storms was not unusual for typical monsoonal precipitation in this region (recurrence interval (RI) < 1 year), but multiday rainfall where slope failures occurred had RI > 50 years and individual grid cells had RI exceeding 1000 years. The 31 July storms caused the watersheds to be essentially saturated following 4 days of rainfall.

Citation: Griffiths, P. G., C. S. Magirl, R. H. Webb, E. Pytlak, P. A. Troch, and S. W. Lyon (2009), Spatial distribution and frequency of precipitation during an extreme event: July 2006 mesoscale convective complexes and floods in southeastern Arizona, *Water Resour. Res.*, *45*, W07419, doi:10.1029/2008WR007380.

1. Introduction

[2] During the week of 27–31 July 2006, an upper level area of low pressure stalled over the four corners region of the southwestern United States. Combining with an unusually moist air mass advected north from the Gulf of California, this low-pressure system promoted the nightly formation of strong mesoscale convective systems (MCSs) over southeastern Arizona, particularly north of Tucson (Figure 1). Over a 5-day period, these systems generated 200–270 mm of rain in a region where annual rainfall is 300–750 mm. Flooding was widespread and stage records were broken at five U.S. Geological Survey (USGS) streamflow gauging stations with return periods estimated in excess of the 100-year flood in the greater Tucson metropolitan area. The extremity of the rainfall was best expressed, however, by the initiation of 435 slope failures and subsequent debris flows [*Magirl et al.*, 2007; *Webb et al.*, 2008] in the Santa Catalina Mountains of southeastern Arizona (Figure 1). This is an area where less than 20 debris flows are known to have occurred historically.

[3] In this paper, we use high-frequency weather radar data calibrated with local point observations of rainfall to estimate grid cell rainfall totals and return periods for the events of 27–31 July 2006 in the Santa Catalina Mountains. We investigate the synoptic weather conditions that promoted the repeated, nightly formation of MCSs over southeastern Arizona, and we analyze the quantity and timing of heavy rainfall over the Santa Catalinas with a focus on the rainfall amounts and frequency that triggered the slope failures and debris flows.

2. Setting

[4] The Santa Catalina Mountains are a metamorphic core complex typical of the Basin and Range Province of North America, and the bedrock of the southern half of the range is almost entirely granitic [*Force*, 1997]. Elevation ranges from 805 m at the mountain front at Sabino Canyon to 2800 m at Mount Lemmon, the tallest peak in the range (Figure 1). The east and west branches of upper Sabino Creek, the principal drainage on the south side of the Santa Catalinas, separate a distinct forerange from the bulk of the mountains to the north. Many smaller canyons drain the forerange from north to south. Most of the mountains are managed as part of the Coronado National Forest, the southern border of which follows the sharply defined mountain front and forms an abrupt transition between the Pusch Ridge Wilderness and metropolitan Tucson (Figure 1).

[5] The climate is semiarid across most of the Santa Catalinas, with mean annual precipitation ranging from 330 mm at the mouth of Sabino Canyon to 750 mm on Mount Lemmon. As in the rest of southern Arizona, precipitation in Tucson is generally biseasonal with maxima in winter and summer. About 45% of rainfall falls during the summer monsoon season of July through September,

[1] U.S. Geological Survey, Tucson, Arizona, USA.
[2] U.S. Geological Survey, Tacoma, Washington, USA.
[3] NOAA/National Weather Service, Tucson, Arizona, USA.
[4] Hydrology and Water Resources, University of Arizona, Tucson, Arizona, USA.
[5] Physical Geography and Quaternary Geology, Stockholm University, Stockholm, Sweden.

0043-1397/09/2008WR007380$09.00

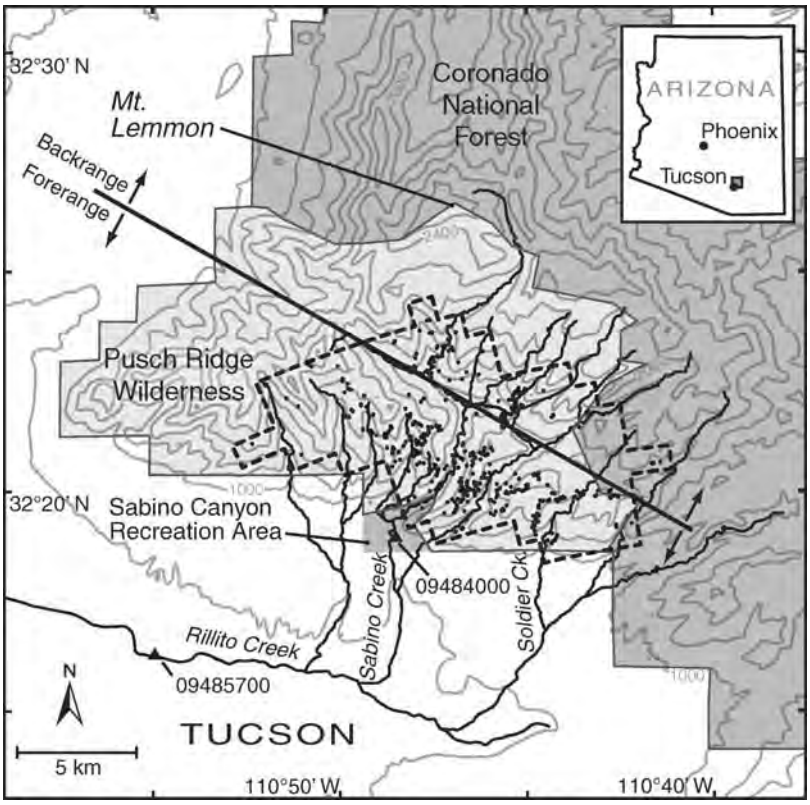

Figure 1. Map of study area north of Tucson, Arizona, indicating general topography of the Santa Catalina Mountains, major southern drainages, and locations of 435 slope failures that occurred on 31 July 2006. The failure zone is outlined with a dashed line. USGS gaging stations at Sabino Creek (09484000) and Rillito at Dodge (09487500) are indicated with black triangles. The Coronado National Forest and Pusch Ridge Wilderness areas are indicated with dark and light gray shading, respectively. Contour interval is 200 m.

typically in convective storms, and about 34% of precipitation occurs between December and March during less intense storms [*Green and Sellers*, 1964].

2.1. Flood Hydrometeorology of Southern Arizona

[6] Flood-producing storms in southern Arizona have been categorized as (1) frontal and(or) cutoff low-pressure systems that occur most often in fall, winter, and spring; (2) dissipating tropical cyclones advecting moisture in the region in the summer and fall; and (3) monsoonal storms typically of local extent affecting the region from late June to September [*Webb and Betancourt*, 1992]. Smaller drainages tend to be most affected by locally intense summer thunderstorms; during the North American Monsoon, severe thunderstorms with heavy rainfall are common [*Maddox et al.*, 1995].

[7] Although more rare, mesoscale convective systems (MCS) have been recognized as important in generating floods during the summer [*Hirschboeck*, 1985]. Numerous large MCS storms in Arizona have been documented [*Hales*, 1975; *McCollum et al.*, 1995; *Maddox et al.*, 1995]. The synoptic features promoting formation of these extreme precipitation events in Arizona are common to heavy rainfall events elsewhere in the world and include high surface dew points, large moisture content throughout the atmospheric column, and weak to moderate vertical wind shear [*Maddox et al.*, 1979]. In addition, the presence of a strong near-surface jet of moist air impinging on a mountain front is now recognized as a significant contributing factor to many extreme rain-producing storms in complex terrain [*Landel et al.*, 1999].

[8] In Arizona, surges of moist air from the Gulf of California can enhance monsoonal activity [*Douglas*, 1995], and these surges have also been directly linked to instability and the formation of severe thunderstorms [*McCollum et al.*, 1995]. Recently, the role of subtropical upper tropospheric lows (upper level low) or inverted troughs in modulating the coverage and intensity of MCSs in the monsoonal patterns has been recognized [*Pytlak et al.*, 2005]. These usually weak, upper level areas of low pressure (upper level lows) often sweep westward across Arizona during the monsoon, promoting the formation of MCSs. Sinking air at the upper level low tends to suppress convection while the instability tends to promote strong convective activity on the periphery of the low; the convection tends to form toward the west of the low exacerbated by instability from the mountain ranges in the Southwest.

2.2. July 2006 Floods and Debris Flows

[9] On 31 July 2006, record floods occurred in several drainages from the Santa Catalina and Rincon Mountains north and west of Tucson, including Sabino Creek (09484000, 75-year record), which had a peak discharge of 445 m^3/s and

Rillito Creek (09486000 and 09485700, combined 87-year record), which had a peak discharge of 1070 m^3/s. The floods on Sabino and Rillito Creeks both had recurrence intervals (RI) > 100 years for the respective gauging records before 2006 [*Pope et al.*, 1998].

[10] In addition, 435 slope failures occurred in a 100 km^2 region in the forerange of the Santa Catalina Mountains (Figure 1). The Santa Catalina Mountains received heavy rainfall nightly throughout the period of 27–31 July, culminating with a particularly prolonged and heavy MCS that repeatedly formed over the forerange from 00:00 to 08:00 A.M. MST on 31 July. Some of the slope failures coalesced into debris flows, five of which reached or exited the mountain front onto alluvial fans. At least 13 debris flows caused significant damage to the Sabino Canyon Recreation Area (U.S. Forest Service) and other properties in metropolitan Tucson [*Magirl et al.*, 2007].

[11] Debris flows in the Santa Catalina Mountains are historically rare, although they are known to have occurred following wild land fires in southeastern Arizona [*Wohl and Pearthree*, 1991; *Schaffner and Reed*, 2005]. Before 31 July 2006, fewer than a dozen debris flows have been recorded in the Santa Catalina Mountains (P. A. Pearthree, written communication, 2006). The slope failures of July 2006 in these mountains occurred almost exclusively in the Pusch Ridge Wilderness, an area largely unaffected by land use practices except wild land fire. In 2003, the Aspen Fire burned 337 km^2 of the Coronado National Forest, including 86% of the area within which slope failures occurred. However, based on the morphology of the slope failures, the 3-year time interval between the fire and the failures, and the fact that most slope failures occurred in unburned or low-intensity burned sites, the Aspen Fire is not believed to be the general cause of the July 2006 slope failures [*Magirl et al.*, 2007; *Webb et al.*, 2008]. Instead, we hypothesize that extreme, multiday precipitation is the reason for the spate of slope failures.

3. Methods

3.1. Synoptic Weather Patterns

[12] The overall daily weather maps for 27–31 July 2006 at the surface and 500-mb heights are available at http://www.hpc.ncep.noaa.gov/dailywxmap/index_20060727.html. Much of the atmospheric data in the study were collected at the time of the event by the National Weather Service (NWS) Weather Forecast Office in Tucson, Arizona. Upper air soundings at Tucson were taken daily at 5:00 A.M. MST (12:00 UTC) and 3:00 P.M. MST (0:00 UTC) and report winds, precipitable water, and atmospheric convective instability. Precipitable water is a measure of the total atmospheric water contained in the air column of the sounding. The convective available potential energy (CAPE) is reported to indicate the tendency of the atmosphere to support free convection (http://www.tornadochaser.net/cape.html). Archives of soundings are available from the University of Wyoming, and the upper level analyses were retrieved from the NWS archives as well as the daily weather map archive.

3.2. Rainfall Data

[13] Rain gauge data were obtained from 31 stations in the study area in operation during July 2006. Eight of these are long-term stations maintained by Pima County Regional Flood Control District as part of its ALERT system (http://rfcd.pima.gov/alertsys/index.cfm). Three ALERT stations were situated at the top of the Santa Catalina Mountains between 2560 and 2740 m elevation, and five stations were located along the mountain front between 570 and 1170 m elevation. These eight stations with tipping bucket gauges, measuring in 1 mm increments, surround the area where slope failures occurred.

[14] In addition, 24 temporary rainfall gauges established by the University of Arizona also collected data in the study area in July 2006. Most (21) of these gauges were clustered along ridge tops within 4 km of Mt. Lemmon (2230 to 1760 m elevation), but two (gauges 14 and 15) were located in the middle of the slope failure zone (1121 and 1128 m elevation). These gauges were also tipping bucket gauges with 0.254 mm resolution recording at 1-min intervals that were summed and recorded in 15-min increments. The ALERT station data were resampled to conform to 15-min increments.

3.3. Weather Radar

[15] Despite the large number of rainfall gauges in the study area, only two were in the area where slope failures occurred (Figure 2). In order to map the spatial distribution of rainfall in greater detail, particularly across the failure area, we analyzed weather radar data collected by radar site KEMX, located approximately 40 km southeast of Tucson at the north end of the Empire Mountains (1586 m elevation). This installation has a relatively direct view of the Santa Catalina Mountains unimpeded by intervening topography and provides complete coverage of the study area. Using base reflectivity data, KEMX radar coverage provides continuous data in the form of mean areal estimates over approximately 1 km^2 grid cells in 5-min intervals. Using point rainfall data from the 31 rain gauges, we calibrate a radar rainfall relation specific to the 5 days of rainfall in the study area and estimate radar rainfall amounts accordingly.

3.3.1. Radar Reflectivity Data

[16] Radar reflectivity data are measures of the radar energy backscattered by the cross-sectional area of hydrometeors (e.g., raindrops, hail) encountered in a given volume of atmosphere. This measure can be correlated with the volume of hydrometeors present in that volume of atmosphere at the time of measurement. Base reflectivity data for this event is available from the National Climatic Data Center (http://www.ncdc.noaa.gov/oa/radar/radardata.html) for atmospheric volumes defined in 0.95° vertical (beginning at 0.5° above the horizontal), 1° horizontal, and 1 km radial increments relative to the radar location. Using this spatial framework, we delineated a horizontal study area 29° wide (azimuth 331° to 360°) by 26 km deep (42 to 68 km from the radar station) over the Santa Catalina Mountains (Figure 2). This defined a grid of 754 radar cells over an area of 722 km^2. At this distance from the radar station, cell area ranges from 0.74 km^2 in the nearest radial to 1.2 km^2 in the most distant radial with a mean cell area of 0.96 km^2, or grid cells approximately 1 km by 1 km. Similarly, cell volumes range from 0.55 to 1.4 km^3 with an average volume of 0.98 km^3.

[17] We downloaded archived data for 27–31 July 2006 and extracted base reflectivity data for the two lowest levels

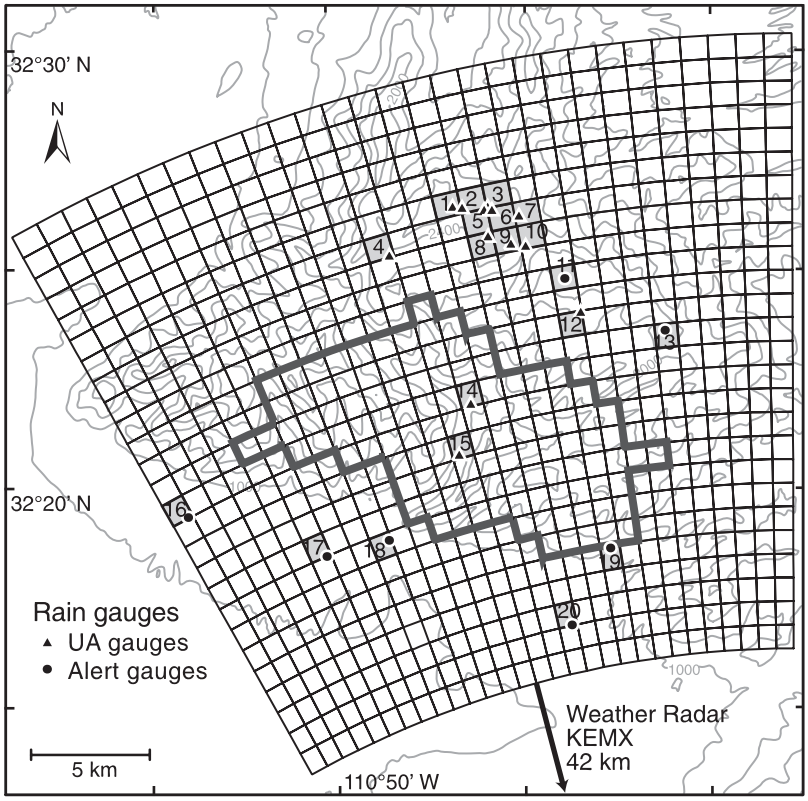

Figure 2. Map of study area north of Tucson, Arizona, showing 754 cells from weather radar KEMX 42 km to the south-southeast and locations of 20 rain gauges (triangles). The slope failure zone is outlined in black, and the contour interval is 200 m.

of scan (level 0 from 0.5 to 1.45°, and level 1 from 1.45 to 2.4°). All reflectivity values were converted from dB to standard units of reflectivity (mm^6/m^{-3}) for all computations and evaluations. Missing reflectivity values were estimated as the average of the immediately preceding and following values for that grid cell. For grid cells in the study area that overlay rain gauges, we compared the time series of radar reflectivity from both scan levels to the time series of point precipitation to evaluate the presence of any time lag between radar and rain gauge measurements.

[18] Ideally, the lowest-elevation radar data (level 0) would be expected to most closely mirror rainfall at ground level. However, given the mountainous terrain, the lowest-level data may be severely affected by ground clutter (the distortion of the radar signal through interaction with features on the ground surface) and other negative effects due to the proximity of the ground surface. We evaluated both level 0 and level 1 data for potential interference with the landscape, compared variation in reflectivity between the two layers of data, and determined whether to use one particular level or a combination of the two.

3.3.2. Local Z-R Relation

[19] Although there are a variety of ways to relate the radar reflectivity factor (Z, mm^6/m^3) to rainfall intensity (R, mm/h), the most common method is a simple power law relation:

$$Z = A \cdot R^b. \quad (1)$$

A broad range of values for coefficients A and b have been derived worldwide from a variety of data sets [*Stout and Mueller*, 1968; *Battan*, 1973; *Raghavan*, 2003]. The variation in calculated Z-R relations derives from the fact that the radar reflectivity factor is essentially a measure of the surface area of hydrometeors facing the radar antenna. A stable Z-R relation assumes a constant drop-size distribution (DSD) and fall velocity and thus a constant relation between surface area and rain volume. DSD is demonstrably not stable; it can vary with climatic region, local topography, season, and storm type [*Stout and Mueller*, 1968; *Nicholas and Larkin*, 1976; *Joss and Waldvogel*, 1989]. DSD often varies temporally and spatially within a single storm as well [*Cataneo and Stout*, 1968; *Carbone and Nelson*, 1978]. This variability is reflected in the five different Z-R relations recommended by the NWS for analysis of WSR-88 radar data depending on storm type and geographic region [*Belville*, 1999].

[20] Given the potentially poor fit of existing Z-R relations, we elected to directly estimate a Z-R relation based specifically on radar rainfall data from within the study area. One benefit of this approach is that we do not need to evaluate the potential of local variation in radar reflectivity with altitude, a vertical profile of reflectivity (VPR). By ignoring a possible VPR, we calculate essentially a locally unique Z-R relation that is not comparable to other Z-R relations. This step simplifies the calculation of the Z-R relation considerably. Z-R relations are known to scale with temporal and spatial intervals: as data is integrated over time and/or space, scatter declines and model fit improves

[*Morin et al.*, 2003], and it is common practice to evaluate Z-R relations for hourly rainfall. However, because we are interested in evaluating spatial and temporal variability within the storms at the highest possible resolution, we elected to calibrate Z-R relations for both 15- and 60-min time intervals, averaging 5-min base reflectivity (mm^6/m^3) and 15-min gauge rainfall (mm/h) data accordingly.

[21] Where multiple rain gauges occur beneath a single radar cell, the gauge data were averaged into one mean rainfall value for that cell, reducing the number of effective gauges from 31 to 20 (Figure 2). The 15-min relation was used to estimate radar rainfall of 5- and 15-min durations, while the 60-min relation was used to estimate rainfall of 60-min durations. Rainfall over 1-, 2-, 4-, and 5-day durations was estimated by summing 60-min estimates. Z-R relation parameters were estimated by adjusting b and A in an iterative manner (modeling R on Z) to minimize the mean squared difference between measured (rain gauge) and modeled (radar) rainfall intensity [*Ciach and Krajewski*, 1999].

3.4. Rainfall Depth, Intensity, and Recurrence Intervals

[22] Mean rainfall estimates for a variety of recurrence intervals and durations over the study area were taken directly from the National Oceanic and Atmospheric Administration (NOAA) Atlas 14: Precipitation-Frequency Atlas of the United States (available at http://hdsc.nws.noaa.gov/hdsc/pfds/index.html) [*Bonnin et al.*, 2006]. These estimates are derived from rain gauge records using the method of L-moments to define regional probability distributions; these distributions are then scaled with estimates of mean annual maximum precipitation to calculate quantiles at specific points in space. We downloaded these frequency estimates as georeferenced raster data with a resolution of approximately 0.7 km^2 in the Tucson area. This provided slightly more than one frequency estimate (the center of the frequency grid cell) for a given duration over each weather radar cell in the study area. For any given cell, we selected the frequency data from the NOAA atlas data point closest to the center of the cell. These data were then used to assign mean rainfall recurrence intervals to rainfall totals at 5-min, 1-day, 2-day, 4-day, and 7-day durations for each radar cell and corresponding rain gauge in the study area.

[23] By applying these frequency estimates to weather radar cells, we necessarily mix point data with mean areal data. In a fully rigorous approach, these two data types are not directly comparable; the point data can be no better than a sample of the population of which the areal measure is a mean, and we cannot be sure if that sample is above or below the mean, let alone its deviation. One common practice in extrapolating point rainfall data over large areas (>10 km^2) is to apply an Areal Reduction Factor (ARF) to the rainfall value [e.g., *Zehr and Meyers*, 1984]. However, for the relatively small area represented by the weather radar cells (1 km^2), any ARF applied would approach unity and make any adjustment to the point estimates negligible. On this basis we have elected to directly compare point rainfall frequency with radar rainfall estimates for radar cells. Given that mean areal rainfall across large areas is typically lower than at a single gauge (as is suggested by the ARF approach), any error arising from this comparison is likely to result in an underestimation of recurrence intervals for the radar-based rainfall.

3.5. Sabino Creek Hydrology

[24] We compared runoff in Sabino Creek to the input rainfall to determine the runoff coefficients associated with the 27–31 July 2006 storms. The USGS gauging station "Sabino Creek near Tucson, Arizona" (09484000, Figure 1) recorded stage at 15-min intervals during the July 2006 floods. The gauging station is at an elevation of 829 m, and the watershed above the station drains 91.9 km^2 in the center of the area of slope failures and heavy precipitation. The station is upstream from a stable, sediment-filled dam and reports reliable, unshifting stage data, even during floods. A postflood indirect discharge estimate established the peak discharge of the flood and allowed scaling of the stage discharge relation for high flow, which cannot be directly measured at this site. The total depth of runoff from the drainage, r_d, was calculated by dividing the total volume of flow measured at the gauging station by the total drainage area.

[25] To determine the total areal depth of rain gauge-measured rainfall within the limits of the Sabino Creek watershed, Thiessen polygons [*Linsley et al.*, 1982] were used to weight by area the rainfall contribution from the 14 rainfall gauges located within the drainage. The total average areal rainfall, R_m, represented the area-weighted mean of the 14 gauges:

$$R_m = \frac{1}{A}\sum_{i=1}^{N} A_i P_i, \tag{2}$$

where A is the total area of the drainage, A_i is the sub area of each Thiessen polygon, and P_i is the rainfall measured by the rain gauge in each polygon. Radar-based areal rainfall estimates were also calculated by summing rainfall depths in all radar cells and fractions of radar cells that fall within the boundaries of the Sabino Creek drainage above the stream gauge.

[26] Daily runoff coefficient, C, was calculated by dividing the total depth of runoff, r_d, by the total depth of rainfall, R_m, in the drainage on each day:

$$C = \frac{r_d}{R_m}. \tag{3}$$

The Sabino Creek drainage is small and base flow is negligible compared with storm runoff (discharge averaged 0 m^3/s on 26 July 2006), and essentially the entire discharge of the hydrograph over a 24-h period starting from the beginning of the rise of a flood was considered storm runoff.

4. Results

4.1. Synoptic Conditions

[27] Monsoonal rain in southeastern Arizona started in late June 2006 and typical local thunderstorms occurred over the following weeks. A marked increase in storm activity occurred on 25 July as the remnants of Tropical Storm Emilia moved northward from the eastern Pacific Ocean. Precipitable water values at Tucson reflected this

moisture increase on 25 July and show trends of increasing moisture into the last week of July.

[28] Beginning on 27 July, a subtropical upper tropospheric low (upper level low) stalled over the Four Corners region of the southwestern United States, and wind vectors measured at Flagstaff and Phoenix show southerly flow aloft that persisted for the next four days. During the North American Monsoon, about 20–25 upper level lows and waves commonly sweep across Arizona, triggering increased thunderstorm and potential MCS activity [*Pytlak et al.*, 2005], but it is unusual for an upper level low to stall and influence the region for several days. Though not explicitly tracked in the meteorological records, our review of the data suggests that the late July 2006 incident was the first time in a decade that an upper level low stalled in the Four Corners Region during the monsoon.

[29] Simultaneously, a humid air mass moved northward from the Gulf of California over Arizona and New Mexico and was resupplied with surges throughout the week. As the moist air rotated around the upper level low, MCSs formed nightly over the central highlands of eastern and north central Arizona and were steered into southeastern Arizona by the persistent upper level winds during the early morning hours, resulting in heavy, sustained periods of thundershowers in southeastern Arizona. Conditions of moderate and southerly wind shear remained throughout the week, differing markedly from the light upper level steering winds typical of extreme storms elsewhere in the United States [*Maddox et al.*, 1979].

[30] In the early morning hours of 27 July, an MCS moved into the Tucson region from the northeast, generating 12–50 mm of rainfall over the Santa Catalina Mountains. The convective available potential energy (CAPE) for the 4:00 P.M. MST 27 July sounding was 454 J/kg, indicating modest convective potential. Another MCS moved over the Santa Catalinas from the northeast in the early morning hours of 28 July, resulting in a CAPE of 190 J/kg and rainfall of 15–30 mm. The wind pattern changed slightly in the early morning hours of 29 July as the winds aloft shifted to north by northwest, steering still stronger MCSs into southeastern Arizona. Air mass instability increased as CAPE rose to 892 J/kg, and rainfall on 29 July was between 70 and 120 mm. Storm activity on 30 July lessened and rainfall ranged from 15 to 40 mm in the early morning hours, although CAPE remained high at 835 J/kg.

[31] Upper air analysis at 300-mb height showed the closed height contour, upper level low centered over New Mexico on the afternoon of 30 July and a low-pressure trough approaching from the northwest. These two atmospheric features created a divergence zone of upper level instability over Arizona that focused the steering winds directly into southeast Arizona from the northwest. Regions of enhanced convection tend to occur on the southwestern periphery of upper level lows [*Pytlak et al.*, 2005], and that region became centered over southeastern Arizona at about this time.

[32] On the morning of 31 July, MCSs moved from the Phoenix area into southeast Arizona from 00:00 to 8:00 A.M. MST. As the thunderstorms moved over the Santa Catalina Mountains, upper level divergence promoted additional convection. At low levels, a southwesterly low-level jet (30–35 km/h) fed warm, moisture laden air into the mountain range, and southwest trending canyons on the forerange forced those moisture-laden winds to rise and converge on the steep terrain. Later soundings at 05:00 A.M. MST on 31 July showed precipitable water (P_{wat}) at 52 mm, indicating an extremely moist, nearly saturated atmosphere; the 30-year mean P_{wat} for July in Tucson is 32 mm and mean P_{wat} plus two standard deviations is 46 mm. The soundings also measured a CAPE of just 40 J/kg, indicating that the atmosphere had stabilized considerably. However, there were no temperature inversions aloft to impede or prevent convection.

[33] The disturbances rotating around the upper level low created nearly continuous rainfall in the Santa Catalina Mountains for 8 h, but two clearly separable MCSs produced much of the precipitation. The first had a cold cloud top structure (−74°C) that produced heavy, intense rainfall peaking around 03:00 A.M. MST. The second MCS had a warmer cloud top structure (−55°C) and produce less intense but prolonged rainfall from about 05:00 through 08:00 A.M. MST. Warm-top storms efficiently convert atmospheric moisture into rainfall and are associated with extreme flood generation [*Landel et al.*, 1999]. Rainfall totals in the southern Santa Catalina Mountains ranged from 25 to 144 mm on 31 July, with the highest totals centered on the forerange between Sabino and Soldier Creeks (Figure 1).

4.2. Spatial Analyses of Weather Radar Data

4.2.1. Evaluation and Selection of Radar Reflectivity Data

[34] Analysis of the two lowest radar scans with relation to topography indicate that the Santa Catalinas intrude into the level 0 scan at elevations above 2000 m, while the bottom of the level 1 scan clears the top of the mountain range with 420 m to spare. When reflectivity values for the two layers are compared, the values of the level 0 cells are 25 to 125% greater than those of the level 1 cells in a 9-km-deep band between 2000 m elevation and the mountain front. Although the mountains do not physically intrude into the lower radar scan in this band, the high reflectivity values are indicative of the effects of anomalous propagation, in this case the influence of proximal landscape features through downward refraction of the radar beam. This interference is not evident in the level 1 data. Given the corruption or total absence of reflectivity data in 604 of 754 cells (80%) in level 0, we elected to only use the data from level 1 in our analyses. This agrees broadly with the analysis of KEMX data by *Krajewski et al.* [2006], who found considerable beam blockage over the Santa Catalina Mountains in level 0 but not in level 1. When the level 1 reflectivity values are compared as a time series against the 20 sets of rain gauge data, reflectivity peaks match precipitation peaks with no time lag between the two. This suggests that any time lag between rain detected in the atmosphere and rain collected in the rain gauge was smaller than the 15-min sampling interval.

[35] We evaluated the reflectivity data in level 1 for other potential problems inherent to weather radar data, such as the presence of hail, snow, or range effects. There are no obvious outliers in the reflectivity data, and high values cluster at the same time period with other values of similar magnitude, suggesting that hail was not significant. Peak reflectivity values reached 60 to 65 dB on 210 occasions during the week. Level 1 cells reach a maximum altitude of

Table 1. Local Z-R Relation Parameters for 27–31 July 2006

	Parameters		Data Pairs	Error	
Rainfall Duration	*b*	*A*	*n*	RMSE[a]	R^2
15-min	2.6	17	6270	4.7	0.38
60-min	1.9	101	1961	3.0	0.63

[a]RMSE is in mm/h.

4500 m at the northern edge of the study area, while level 1 cells in general average 4000 m; these elevations are well below the 0° isotherm recorded by the NWS rawinsonde at 5000 m altitude on 31 July. This indicates that level 1 data should be unaffected by anomalously high reflectivity from mixed-phase precipitation in the melting layer. Range effects on reflectivity data typically occur with increasing distance from the radar station as larger volumes are sampled at increasingly higher altitudes, and distant samples of larger atmospheric volume and higher altitude may not be comparable to closer distance samples within the same scan layer. Given the relatively small size of the study area (26 cells deep) and its proximity to the radar (<70 km), range effects on this data likely are insignificant. We did not specifically evaluate for the effects of VPR, but the disruption of the level 0 data may be indicative of its effect.

4.2.2. Local Z-R Models

[36] The Z-R models calculated for 15- and 60-min rainfall intervals over the study area for precipitation during 27–31 July 2006 are presented in Table 1. As expected, the 60-min relation was a better fit to the data, which had less scatter than the 15-min data (Figure 3). It is interesting to note that the *b* parameters fall within the range of values calculated by *Morin et al.* [2003] at 15- and 60-min durations for a series of storms in 1999 and 2000 over Walnut Gulch, some 50 km to the southeast of station KEMX.

[37] The low R^2 values and broad scatter of data in Figure 3 should not be interpreted as suggesting that the locally derived Z-R relations poorly estimate rainfall in each radar cell. Rain gauge and radar data are two distinctly different measures taken within the area of a radar cell; a rain gauge samples a point while the radar data estimates rainfall over the entire cell. The link between the spatial variability of precipitation within a storm [e.g., *Nicholas and Larkin*, 1976; *Crane*, 1990; *Goodrich et al.*, 1995] and the high variability between individual gauge measures and radar-based rainfall estimates has been well established [e.g., *Zawadzki*, 1973; *Ciach and Krajewski*, 1999]. *Kitchen and Blackall* [1992] have demonstrated that the relative root mean squared difference between point and mean areal average hourly rainfall can be as high as 150% for convective storms in the United Kingdom.

[38] Sophisticated statistical procedures have been developed to separate the actual radar mean rainfall error from the point area bias in radar rainfall analyses [*Ciach and Krajewski*, 1999; *Anagnostou and Krajewski*, 1999], but these lie beyond the scope of this paper. To evaluate model accuracy, we compared model estimates from each model to the mean and standard deviation of four rain gauges located within a single radar cell (Figure 4). Model estimates for this cell fell within one or two standard deviations of the mean gauge value 69% and 84% of the time, respectively; when model estimates vary by more than one standard deviation from the mean gauge value, that variation averages 1.5 mm/h. These results suggest that most of the variability represented by the RMSE and R^2 measures reflects the variability of point rainfall within a single radar

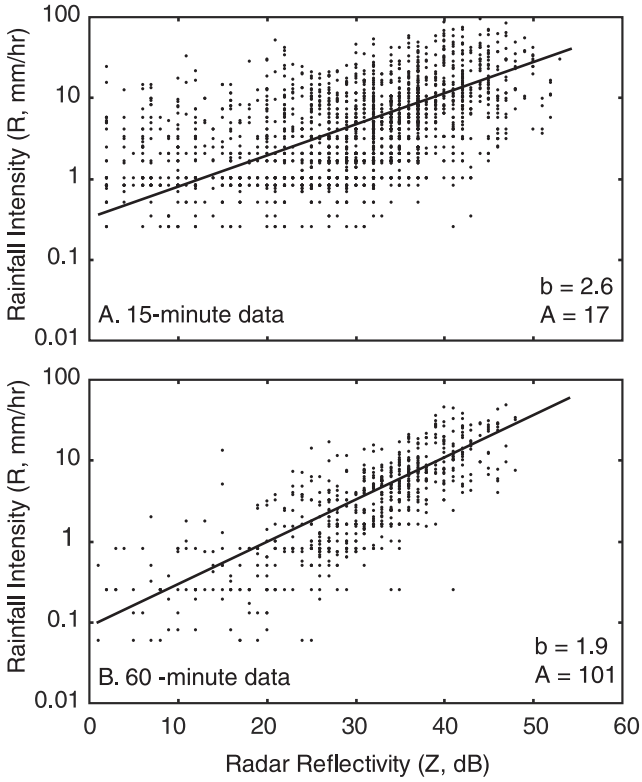

Figure 3. Plots of radar reflectivity versus rainfall intensity along with associated Z-R relations at 15- and 60-min intervals for rainfall over the Santa Catalina Mountains during 27–31 July 2006 (see Table 1). The solid black line is a Z-R relation derived specifically for the data using the parameters indicated.

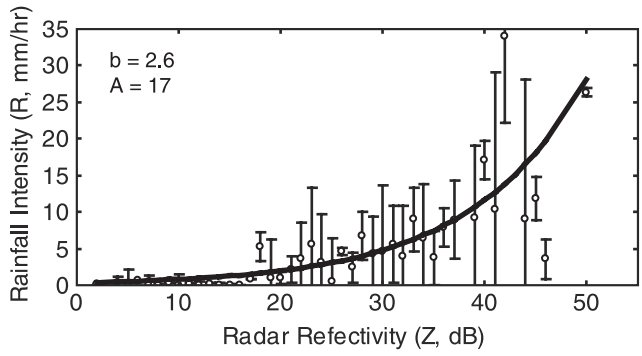

Figure 4. Plot of mean and standard deviation rainfall intensity at 15-min intervals for four rain gauges in one radar cell (gauge 9 in Figure 2) compared with the locally derived Z-R relation (see Table 1). The model falls within 1 standard deviation of the gauge data 69% of the time and within an average of 1.5 mm/h of the gauge mean for the remainder of the data.

Table 2. Mean Rainfall Depth, Intensity, and Recurrence Interval Estimated From Radar Over Different Time Durations for Storms From 27 to 31 July 2006[a]

	All Cells (n = 754)			Failure Zone Cells (n = 113)			Other Cells (n = 641)		
Day/Storm	P (mm)	R (mm/h)	RI (years)	P (mm)	R (mm/h)	RI (years)	P (mm)	R (mm/h)	RI (years)
				5-min Peak					
27	2.3	28	<1	2.3	28	<1	2.3	28	<1
28	2.3	28	<1	2.5	30	<1	2.3	28	<1
29	2.1	26	<1	1.9	23	<1	2.2	26	<1
30	2.0	24	<1	2.3	28	<1	1.9	23	<1
31	1.9	23	<1	2.3	28	<1	1.8	22	<1
				15-min Peak					
27	5.2	21	<1	5.0	20	<1	5.2	21	<1
28	5.0	20	<1	5.4	22	<1	4.9	20	<1
29	5.1	21	<1	4.4	18	<1	5.3	21	<1
30	4.7	19	<1	5.5	22	<1	4.5	18	<1
31	4.5	18	<1	5.5	22	<1	4.3	17	<1
				1-h Peak					
27	14	14	<1	12	12	<1	15	15	<1
28	13	13	<1	14	14	<1	13	13	<1
29	16	16	<1	13	13	<1	16	16	<1
30	13	13	<1	17	17	<1	12	12	<1
31	12	12	<1	17	17	<1	11	11	<1
				1-day Total					
27	43	1.8	1	38	1.6	<1	44	1.8	1
28	33	1.4	<1	33	1.4	<1	33	1.4	<1
29	58	2.4	2	58	2.4	1	58	2.4	2
30	25	1.0	<1	31	1.3	<1	24	1.0	<1
31	48	2.0	1	68	2.8	5	44	1.8	1
				2-day Total					
27–28	76	1.6	5	72	1.5	2	77	1.6	5
28–29	91	1.9	10	92	1.9	10	91	1.9	10
29–30	83	1.7	5	89	1.8	5	82	1.7	5
30–31	73	1.5	2	99	2.1	10	68	1.4	2
				4-day Total					
27–30	159	1.7	50	160	1.7	50	159	1.7	50
28–31	165	1.7	50	190	2.0	100	159	1.7	50
				5-day Total					
27–31	208	1.7	-	229	1.9	-	203	1.7	-

[a]Recurrence intervals are drawn directly from *Bonnin et al.* [2006].

cell rather than the accuracy of the models in tracking mean rainfall within that cell as well as any error in the rain gauge measurement itself.

4.2.3. Radar Rainfall Depth and Frequency

[39] Mean rainfall depth (P) and intensity (R) derived from radar reflectivity data and the associated expected recurrence intervals (RI) are listed in Table 2 for several time durations. Average values are given for all cells in the study area, as well as for only those cells in the slope failure zone and for other cells outside that zone. Rainfall was not extreme at any duration for any single storm; mean peak 5-min, 15-min, and 1-h rainfall depths across the study area had RI < 1 year, and mean storm (1 day) rainfall at best had RI > 2 years (29 July). For 31 July, RI was <1 year for 5-min, 15-min, and 1-h rainfall for every radar cell in the study area. Mean peak rainfall depths for 31 July were 1.9, 4.5, and 12 mm for 5-min, 15-min, and 1-h rainfall durations, respectively.

[40] Comparing individual storms, rainfall during the storm of 31 July was not the most intense at any duration. Peak 5- and 15-min rainfall were greatest on 27 July at 2.3 and 5.2 mm (28 and 21 mm/h), respectively. Peak hourly and total 1-day rainfall were greatest during the storm of 29 July at 16 mm and 58 mm (2.4 mm/h; RI > 2 years). Rainfall on 31 July was actually the lowest at all durations except 1-day, for which it was the second highest rainfall at 48 mm (2.0 mm/h; Figure 5a) and RI > 1 year. One-day rainfall for both 29 and 31 July had maximum RIs > 100 years for some cells within the slope failure zone (Figure 5b).

[41] Extreme levels of rainfall during the final week of July 2006 are evident only when rainfall is aggregated over multiple storms. Two-day rainfall over 28 and 29 July achieves a RI > 10 years (91 mm), while 4-day rainfalls over 27–30 July and 28–31 July both have RIs > 50 years (159 and 165 mm, respectively; Figure 6). Individual radar cells for 4-day rainfall over 28–31 July reach RIs > 200, 500, and even 1000 years (Figure 6b).

[42] The accumulation of rainfall over multiple days had a distinct effect in the net distribution of rainfall across the study area. Although the spatial distribution of rainfall varied for each storm, together they had the net effect of delivering more water inside the slope failure zone (SFZ) than outside (Figure 6). The principle elements of this shift in rainfall toward the SFZ were the delivery of heaviest rainfall (1-day rainfall exceeding 85 mm) to the southwestern corner of the SFZ on 29 July followed by the distribution of heaviest rainfall (1-day rainfall exceeding 60 mm) across the northwest-southeast axis of the SFZ on 31 July.

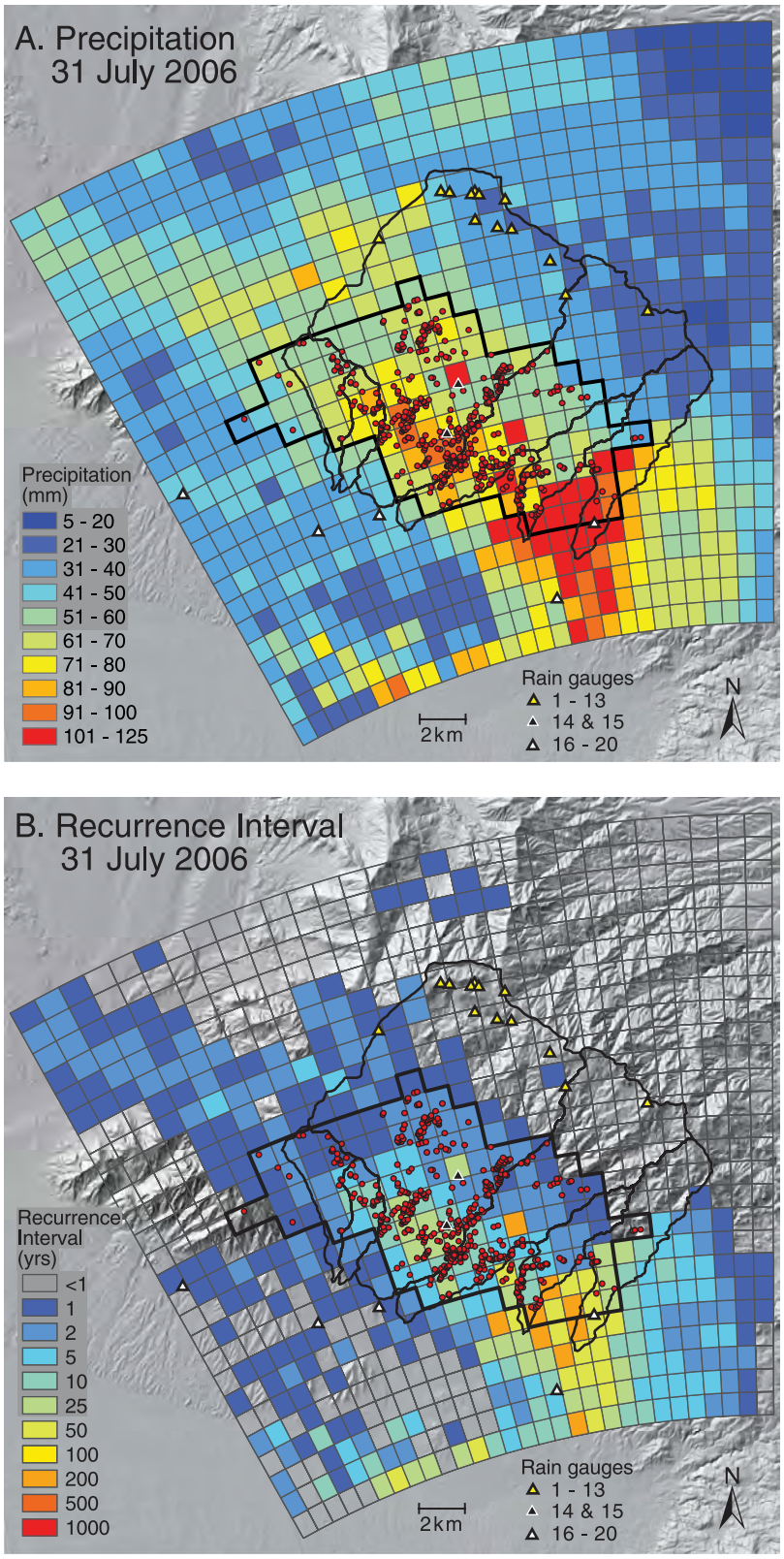

Figure 5. Maps of 1-day rainfall derived from weather radar data for 31 July 2006. Red circles indicate slope failures, and the slope failure zone is outlined in black. (a) Rainfall depth (P) in millimeters (see Animation S1). (b) Recurrence intervals (RI) in years.

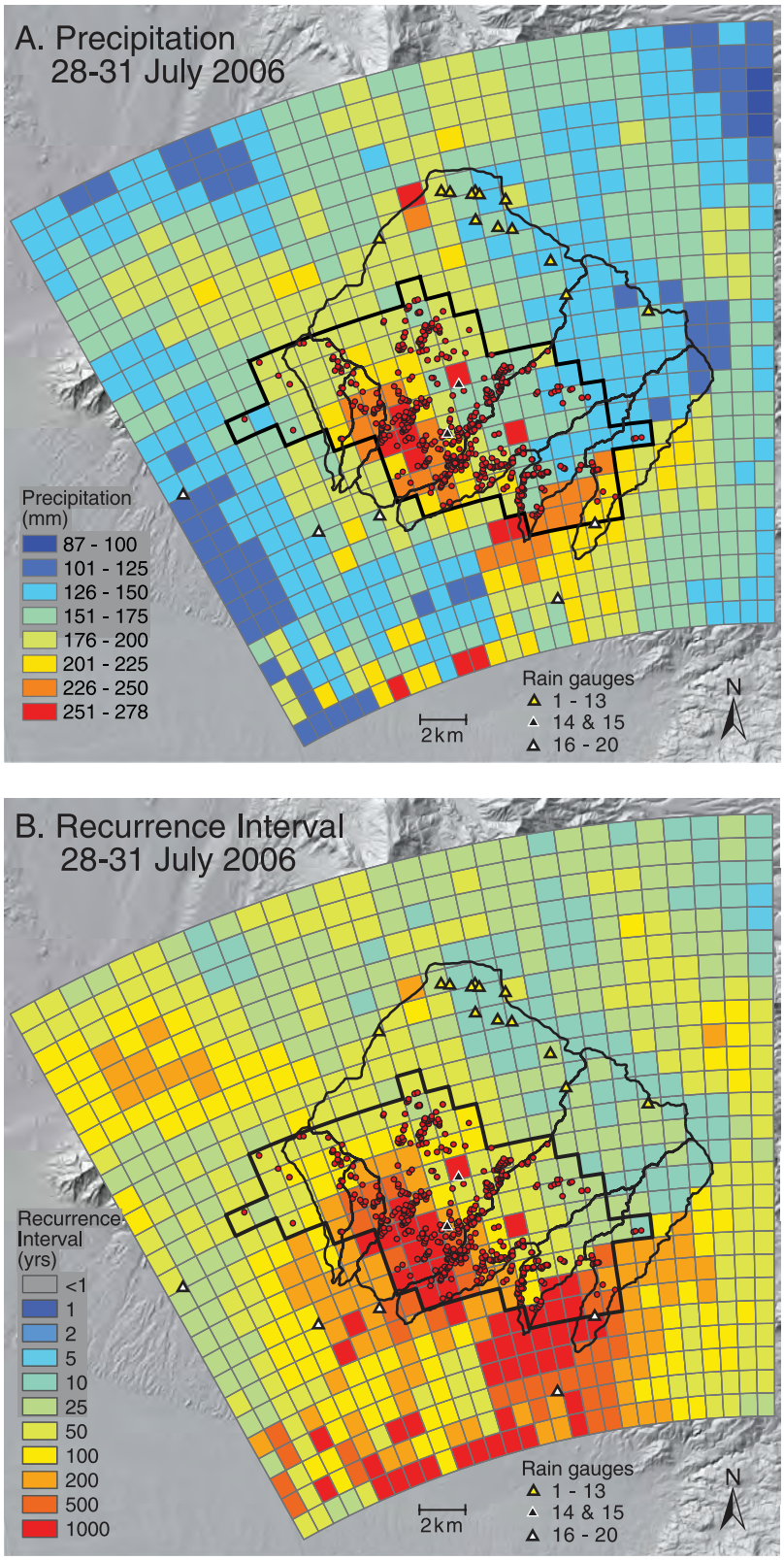

Figure 6. Maps of cumulative 4-day rainfall derived from weather radar data for the period of 28–31 July 2006. Red circles indicate slope failures, and the slope failure zone is outlined in black. (a) Rainfall depth (P) in millimeters. (b) Recurrence intervals (RI) in years.

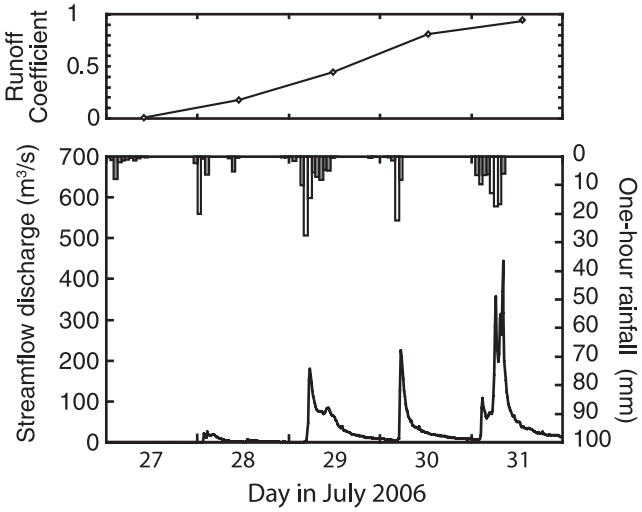

Figure 7. The hydrograph measured at the USGS gaging station Sabino Creek near Tucson, Arizona (09484000). The peak flow of 445 m^3/s occurred at 8:22 A.M. MST 31 July, but multiple peaks in the hydrograph indicate the sustained and widespread nature of the rainfall (solid line). The hyetograph of rainfall within the watershed boundary (bar graph) shows rainfall intensity was never exceptional. Most telling in terms of geomorphic response, the daily runoff coefficient increases steadily from 27 to 31 July, indicated that the soils were nearly saturated on 30 July and 31 July in response to the rainfall of 28 and 29 July.

This pattern of rainfall was particularly influenced by the cold top phase of the storm on 31 July. Although total rainfall from the cold-top phase was less than from the warm-top phase, its distribution was particularly focused within the SFZ (see Animation S1)[1]. The net result is a mean RI > 100 years (100 mm) within the SFZ compared to RI > 50 years (159 mm) outside the SFZ for 4 days of rain. Within the SFZ, 18% of radar cells had RI > 200 years, 13% had RI > 500 years, and 18% had RI > 200 years for this duration of rainfall. There was also a zone of extreme (RI > 500 and 1000 years) 4-day rainfall southeast of the SFZ over relatively flat terrain to the south of the mountains where slope failures would not occur.

4.3. Hydrologic Response of Sabino Creek

[43] Flash flooding in the semiarid, steep terrain of the Santa Catalina Mountains is common, but the flooding that occurred in Sabino Creek on 31 July 2006 was record setting. The USGS gauging station on Sabino Creek has provided a continuous record of streamflow back to 1932 and the 31 July flood of 445 m^3/s is the largest in the 77-year record (the previous record was 436 m^3/s on 15 July 1999). Figure 7 shows the hydrograph at the gauging station over the last five days in July 2006 and the mean areal rainfall, determined as the mean of radar and rain gauge data, over the drainage.

[44] The rainfall from the first MCS on 27 July (27 mm) resulted in no appreciable runoff at the gauging station. The rainfall on 28 July (26 mm) resulted in a peak discharge of 26 m^3/s and a total runoff of 4.6 mm. The mean of rain gauge and radar runoff coefficients from these first two days of rain were C = 0.004 and C = 0.18, respectively, indicating that much of the precipitation was caught in abstractions in the drainage. During the heavy rainfall of 29 July, soils were approaching saturation; 81 mm of rain fell on this day causing a peak discharge of 181 m^3/s, a total runoff of 36 mm, and C = 0.44. By 30 July, C = 0.81, indicating the soil in the watershed were nearly saturated. Indeed, the smaller rainfall of 32 mm on 30 July produced a peak discharge of 225 m^3/s, exceeding the flood of the previous day.

[45] Saturated soil conditions continued into 31 July when 70 mm total rainfall produced a peak discharge of 445 m^3/s. The rainfall, however, was long duration (about 400 min) and thus not particularly intense (about 11 mm/h). Total runoff from the two storms was 66 mm, nearly double the runoff from a similar amount of precipitation two days earlier. With C = 0.94, soil in the Sabino Creek drainage was essentially saturated. This increase in runoff coefficient over the several consecutive days of rainfall is similar to that reported by *Lyon et al.* [2008] for the Upper Sabino catchment nested within Sabino Creek watershed. *Lyon et al.* [2008] observed that the runoff coefficient increased each day following rainfall until reaching a plateau after 29 July. Most summer thunderstorms affecting Sabino Creek are intense and short-lived; the previous record flood in 1999, for example, had a total runoff of only 38 mm for a rainfall depth of 61 mm (C = 0.62). The hydrograph of that 1999 storm rose and fell quickly, with a total volume of discharge roughly half that of the 31 July 2006 storm, and was more comparable to the 29 July 2006 storm.

5. Discussion

[46] Conditions that led to the 31 July floods and debris flows in southern Arizona were similar to other extreme flood-producing storms elsewhere in the United States [e.g., *Maddox et al.*, 1978; *Landel et al.*, 1999] with two exceptions: (1) the upper level steering winds were relatively strong, sweeping MCSs through the region rather than the weak upper level winds in other extreme storms that allowed those storms to remain nearly stationary; and (2) the precipitation responsible for floods and debris flows was the result of multiple MCSs affecting the same region over five consecutive days, instead of the more typical isolated MCS. Unusual atmospheric conditions occurred on 31 July that included an exceptionally moist atmosphere, an upper level divergence, and a strong low-level jet combined to deliver and enhance two major MCSs over the study area. The role of low-level jet in promoting extreme storms has been previously documented along the Mediterranean Sea [*Delrieu et al.*, 2005; *Borga et al.*, 2007], the Appalachian Mountains [*Smith et al.*, 1996; *Hicks et al.*, 2005], and elsewhere in the western United States [*Caracena et al.*, 1979; *Maddox et al.*, 1978; *Petersen et al.*, 1999], but not in southern Arizona. By all measures, the most intense and deepest rainfall did not occur on 31 July, and radar-based estimates of 5-min, 15-min, and 1-h rainfall amounts for all storms indicate that peak intensity was not unusual (typically RI < 1 year). This suggest that the unique trigger of record debris flows and flooding was not the intensity of rainfall on any single day, but the unusual duration of moderate

[1] Auxiliary materials are available in the HTML. doi:10.1029/2008WR007380.

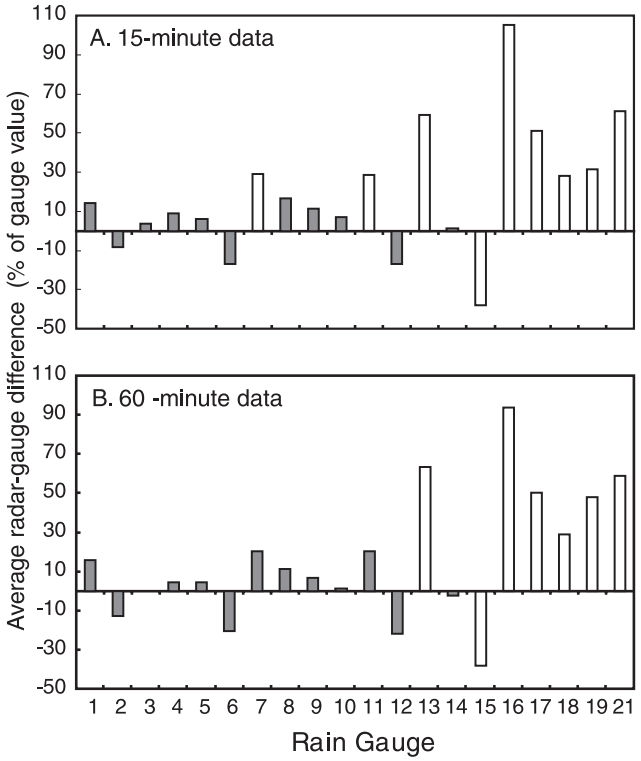

Figure 8. Plots of mean difference between radar-derived and rain gauge–measured rainfall at each rain gauge for the period of 27–31 July 2006. Differences are expressed as a percentage of the rain gauge measured value. Gauges 1–13 are in the mountains between 2300 and 2800 m, gauges 14 and 15 are in the heart of the slope failure zone at 1100 m, and gauges 16–17 are along the mountain front below 1100 m. Radar-derived rainfall estimates underpredict rainfall in the heart of the slope failure zone (gauge 15) by as much as 40% and overpredict rainfall along the mountain front by as much as 20 to 80%.

intensity rainfall delivered by multiple MCSs over several days.

[47] Although some applications of point rainfall recurrence intervals to radar-based rainfall estimates have seen large uncertainties in estimated return periods [*Norbiato et al.*, 2007], the radar rainfall return periods calculated here agree closely with return periods calculated for data from local rain gauges, which ranged from 25 to 900 years for 4-day rainfall [*Webb et al.*, 2008]. However, there is some evidence that the Z-R parameters may underestimate rainfall in some sections of the study area as a result of errors in the radar data. A closer examination of cumulative radar-derived rainfall suggests the possibility of inaccurate radar returns in the eastern half of the slope failure zone (SFZ) as well as along the mountain front to the immediate south. This potential radar artifact takes the form of consistently sharp transitions to low values in the eastern half of the SFZ, then sudden high values along the mountain front. This anomaly is most readily visible when precipitation is summed over several days (Figure 6), but is also apparent in 1-day rainfall maps of 29–31 July (Figure 5). A similar pattern is evident when rain gauge rainfall is compared with associated radar cell rainfall at each gauge in Figure 8. Radar estimates compare favorably with measurements at the rainfall gauges 1–13 at higher elevations but underestimate rain gauge measurements by as much as 40% in the heart of the SFZ (gauge 15), and overestimate measurements by as much as 30 to 90% along the mountain front (gauges 16–20). This error is likely the result of strong reflective gradients over the large inner basin of Sabino Creek and the sharp front of the Santa Catalina Mountains, possibly caused by updrafts and downdrafts during the storms. That these errors seem to be most pronounced during the largest storms on 29 and 31 July, particularly the cold-top storm on 31 July, is consistent with this explanation.

[48] If poor radar returns over Sabino Creek basin consistently underestimate rainfall depths, particularly the larger rainfall values that occur during larger storms, then as much as half of the SFZ rainfall may be underestimated. Significantly, adjusting rainfall depths in the SFZ to account for a 20% deficiency (assuming a 40% deficiency in half the SFZ) has little effect on the shorter-duration rainfalls, as RIs remain <1 year for durations less than 2 days. However, this adjustment does have a significant cumulative effect for longer durations and increases 4-day rainfall intensity from 2.0 mm/h to 2.5 mm/h. This corresponds to RI > 500 year for 4-day rainfall in the SFZ. Correction for an underestimate of 20% in the SFZ would raise these 4-day totals to 197 and 232 mm, with corresponding RI > 200 and 500 years, respectively. Multiple slope failures leading to debris flows likely occurred after hillside sediment was nearly saturated, a result of 4-day precipitation exceeding 197 mm, a 4-day average rainfall intensity of nearly 2.1 mm/h.

[49] Although the 31 July flood on Sabino Creek had an RI > 100 years, more exceptional is the sequence of large floods that occurred on consecutive days. The gradual near-saturation of the drainage basin over four days indicates that these floods cannot be considered independent of one another and illustrates the necessity of viewing them as parts of a complex, multiday event. Viewed in terms of multiday flood volume rather than peak discharge, the four consecutive floods on 28–31 July 2006 delivered 11.4 million m^3 of runoff. This is the largest 4-day flood volume associated with summer convective storms recorded on Sabino Creek, except for the flood volume of 12.5 million m^3 ending on 1 August 2006. The third and fourth highest flood volumes also resulted from this storm following the 4-day periods ending on 2 and 3 August 2006, respectively. This prolonged poststorm runoff reflects the draining of a nearly saturated watershed.

[50] The largest 4-day runoff event from a different storm system in summer was 6.8 million m^3 over the four days ending 8 September 1970, part of record flooding and rainfall delivered by a widespread frontal system fueled by remnants of Pacific tropical storm Norma [*Roeske et al.*, 1978]. The 4-day runoff ending 17 July 1999, which includes the second largest 1-day flood on Sabino Creek (15 July 1999), is only the 10th largest such flood, with a total flood volume of 4.6 million m^3, and resulted from a redeveloping monsoonal thunderstorm over Mount Lemmon. When 4-day runoff volumes from all storm types are considered, the July 2006 floods are exceeded only by floods associated with the storms of January 1993, the result of a persistent series of winter frontal systems [*House and Hirschboeck*, 1997], when a maximum 4-day flood volume

of 13.7 million m^3 occurred during the period ending on 10 January.

6. Summary and Conclusion

[51] On 31 July 2006, 5 days of early morning thunderstorms and intense rainfall culminated in record streamflow floods (RIs > 100 years) and an historically unprecedented concentration of slope failures and debris flows in southeastern Arizona. The fortunate coincidence of extensive rain gauge data and relatively unobstructed weather radar has allowed us to examine the spatial and temporal variability of the precipitation that triggered these events in uncommon detail. Radar-based estimates of 5-min, 15-min, and 1-h rainfall amounts for these storms indicate that peak intensity was not unusual, with average RI < 1 year based on NOAA Atlas 14 rainfall estimates. Although record flooding and debris flows occurred during the 31 July storm, the 29 July storm generated the deepest rainfall, with a 1-day average rainfall depth of 58 mm (2.4 mm/h); even so, RI > 2 years for 1-day rainfall for 29 July. Total 1-day rainfall on 31 July was 48 mm with RI > 1 year.

[52] Expected rainfall recurrence intervals increased markedly as rainfall accumulated over multiple days. For 28–31 July, total rainfall depth over the study area averaged 165 mm (1.7 mm/h) with RI > 50 years. As rainfall accumulated, individual storm distributions, particularly on 29 and 31 July, effectively concentrated maximum rainfall within the zone of slope failures. Within this area, 4-day rainfall totals for 27–30 July and 28–31 July totaled 160 mm (1.7 mm/h) and 190 mm (2.0 mm/h), respectively, which correspond to RI > 50 and RI > 100 years. Considering potential radar underestimates in much of the SFZ, these values may be even higher. Correction for an underestimate of 20% in the SFZ would raise these 4-day totals to 192 and 228 mm, with corresponding RI > 200 and 500 years, and RI > 1000 years for several radar cells. Multiple slope failures leading to debris flows likely occurred after hillside sediment was nearly saturated, a result of 4-day precipitation exceeding 192 mm, a 4-day average rainfall intensity of at least 2 mm/h.

[53] That hillslope soil saturation underlies the cooccurrence of so many slope failures in the Santa Catalinas is supported by an analysis of the Sabino Creek runoff generated by the storms. Although the storm on 29 July delivered the most rainfall to the basin (81 mm), larger flood peaks occurred on the next two days, with the flood of record occurring on 31 July. Analysis of runoff relative to rainfall indicates that only half of the rainfall on 29 July exited the basin, with the remainder presumably saturating the basin sediments. On 31 July, 94% of the 58 mm of rainfall delivered to Sabino Creek exited the basin, showing that hillslopes were nearly saturated by this time. This set the stage for multiple slope failures in the SFZ, triggered by rainfall of average intensity.

[54] In contrast to other extreme rainfall events discussed in the literature in which rainfall is continuous over several hours, the 2006 extreme event in Arizona did not consist of a isolated MCS but instead several MCS occurred on consecutive days and increased soil moisture contents to near saturation on a watershed scale. The synoptic atmospheric patterns represent a continuous, multiday weather system that promoted the daily generation of MCS storms that repeatedly affected the same geographic region. Multiple lines of evidence suggest that the extreme flooding and debris flows resulted the unusually long duration of moderate rainfall during these storms, rather than high-intensity rainfall on a single day.

[55] **Acknowledgments.** We thank NWS meteorologists Craig Shoemaker and Glenn Lader, whose poststorm documentation greatly aided the synoptic discussion. We also thank Jeffrey Kennedy of the U.S. Geological Survey, Evan Canfield of the Pima County Regional Flood Control District, and David Goodrich of the U.S. Department of Agriculture Agricultural Research Service for reviewing the manuscript. Funding for this project was provided by the Pima County Regional Flood Control District, the National Weather Service, and the U.S. Geological Survey.

References

Anagnostou, E. N., and W. F. Krajewski (1999), Uncertainty quantification of mean-areal radar-rainfall estimates, *J. Atmos. Oceanic Technol.*, *16*, 206–215, doi:10.1175/1520-0426(1999)016<0206:UQOMAR>2.0.CO;2.

Battan, L. J. (1973), *Radar Observation of the Atmosphere*, 324 pp., Univ. of Chicago Press, Chicago, Ill.

Belville, J. D. (1999), Recommended parameter changes to improve WSR-88D rainfall estimates during cool season stratiform rain events, *Memo. NWFO WSR-88D*, 3 pp., NOAA Natl. Weather Serv., Silver Spring, Md.

Bonnin, G. M., D. Martin, B. Lin, T. Parzybok, M. Yekta, and D. Riley (2006), *Precipitation-Frequency Atlas of the United States*, vol. 1, version 4.0, *Semiarid Southwest (Arizona, Southeast California, Nevada, New Mexico, Utah)*, pp. 1–62, *NOAA Atlas*, *14*, NOAA, Silver Spring, Md.

Borga, M., P. Boscolo, F. Zanon, and M. Sangati (2007), Hydrometeorological analysis of the 29 August 2003 flash flood in the eastern Italian Alps, *J. Hydrometeorol.*, *8*, 1049–1067, doi:10.1175/JHM593.1.

Caracena, F., R. A. Maddox, L. R. Hoxit, and C. F. Chappell (1979), Mesoanalysis of the Big Thompson storm, *Mon. Weather Rev.*, *107*, 1–17, doi:10.1175/1520-0493(1979)107<0001:MOTBTS>2.0.CO;2.

Carbone, R. E., and L. E. Nelson (1978), The evolution of raindrop spectra in warm-based convective storms as observed and numerically modeled, *J. Atmos. Sci.*, *35*, 2302–2314, doi:10.1175/1520-0469(1978)035<2302:TEORSI>2.0.CO;2.

Cataneo, R., and G. E. Stout (1968), Raindrop-size distributions in humid and continental climates and associated rainfall-rate radar reflectivity relationships, *J. Appl. Meteorol.*, *7*, 901–907, doi:10.1175/1520-0450(1968)007<0901:RSDIHC>2.0.CO;2.

Ciach, G. J., and W. F. Krajewski (1999), On the estimation of radar rainfall error variance, *Adv. Water Resour.*, *22*, 585–595, doi:10.1016/S0309-1708(98)00043-8.

Crane, R. K. (1990), Space-time structure of the rain rate field, *J. Geophys. Res.*, *95*, 2011–2020, doi:10.1029/JD095iD03p02011.

Delrieu, G., et al. (2005), The catastrophic flash-flood event of 8–9 September 2002 in the Gard Region, France: A first case study for the Cévennes-Vivarais Mediterranean Hydrometeorological Observatory, *J. Hydrometeorol.*, *6*, 34–52, doi:10.1175/JHM-400.1.

Douglas, M. W. (1995), The summertime low-level jet over the Gulf of California, *Mon. Weather Rev.*, *123*, 2334–2347, doi:10.1175/1520-0493(1995)123<2334:TSLLJO>2.0.CO;2.

Force, E. R. (1997), *Geology And Mineral Resources of the Santa Catalina Mountains, Southeastern Arizona*, *Monogr. Min. Resour. Sci. Ser.*, vol. 1, Cent. for Mineral Resour., Tucson, Ariz.

Goodrich, D. C., J. Faures, D. A. Woohiser, L. J. Lane, and S. Sorooshian (1995), Measurement and analysis of small-scale convective storm rainfall variability, *J. Hydrol.*, *173*, 283–308, doi:10.1016/0022-1694(95)02703-R.

Green, C. R., and W. D. Sellers (1964), *Arizona Climate*, 503 pp., Univ. of Ariz. Press, Tucson.

Hales, J. E., Jr. (1975), A severe southwest desert thunderstorm: 19 August 1973, *Mon. Weather Rev.*, *103*, 344–351, doi:10.1175/1520-0493(1975)103<0344:ASSDTA>2.0.CO;2.

Hicks, N. S., J. A. Smith, A. J. Miller, and P. A. Nelson (2005), Catastrophic flooding from an orographic thunderstorm in the central Appalachians, *Water Resour. Res.*, *41*, W12428, doi:10.1029/2005WR004129.

Hirschboeck, K. K. (1985), Hydroclimatology of flow events in the Gila River basin, central and southern Arizona, Ph.D dissertation, 335 pp., Univ. of Ariz., Tucson.

House, P. K., and K. K. Hirschboeck (1997), Hydroclimatological and paleohydrological context of extreme winter flooding in Arizona, 1993, in *Storm-Induced Geologic Hazards*, edited by R. A. Larson and J. E. Slosson, pp. 1–24, Geol. Soc. Am., Bolder, Colo.

Joss, J., and A. Waldvogel (1989), Precipitation measurement and hydrology, in *Radar Meteorology*, edited by D. Atlas, pp. 577–606, Am. Meteorol. Soc., Boston, Mass.

Kitchen, M., and R. M. Blackall (1992), Representativeness errors in comparisons between radar and gauge measurements of rainfall, *J. Hydrol.*, *134*, 13–33, doi:10.1016/0022-1694(92)90026-R.

Krajewski, W. F., A. A. Ntelekos, and R. Goska (2006), A GIS-based methodology for the assessment of weather radar beam blockage in mountainous regions, *Comput. Geosci.*, *32*, 283–302, doi:10.1016/j.cageo.2005.06.024.

Landel, G., J. A. Smith, M. L. Baeck, M. Steiner, and F. L. Ogden (1999), Radar studies of heavy convective rainfall in mountainous terrain, *J. Geophys. Res*, *104*, 31,451–31,465.

Linsley, R. K., Jr., M. A. Kohler, and J. L. H. Paulhus (1982), *Hydrology for Engineers*, 3rd ed., 508 pp., McGraw-Hill, New York.

Lyon, S. W., S. L. E. Desilets, and P. A. Troch (2008), Characterizing the response of a catchment to an extreme rainfall event using hydrometric and isotopic data, *Water Resour. Res.*, *44*, W06413, doi:10.1029/2007WR006259.

Maddox, R. A., L. R. Hoxit, C. F. Chappell, and F. Caracena (1978), Comparison of meteorological aspects of the Big Thompson and Rapid City flash floods, *Mon. Weather Rev.*, *106*, 375–389, doi:10.1175/1520-0493(1978)106<0375:COMAOT>2.0.CO;2.

Maddox, R. A., D. F. Chappell, and L. R. Hoxit (1979), Synoptic and meso-α scale aspects of flash flood events, *Bull. Am. Meteorol. Soc.*, *60*(2), 115–123.

Maddox, R. A., D. M. McCollum, and K. W. Howard (1995), Large-scale patterns associated with severe summertime thunderstorms over central Arizona, *Weather Forecasting*, *10*, 763–778.

Magirl, C. S., et al. (2007), Impact of recent extreme Arizona storms, *Eos Trans. AGU*, *88*(17), 191–193, doi:10.1029/2007EO170003.

McCollum, D. M., R. A. Maddox, and K. W. Howard (1995), Case study of a severe mesoscale convective system in central Arizona, *Weather Forecasting*, *10*, 643–665.

Morin, E., W. F. Krajewski, D. C. Goodrich, G. Xiaogang, and S. Sorooshian (2003), Estimating rainfall intensities from weather radar data: The scale-dependency problem, *J. Hydrometeorol.*, *4*, 782–797, doi:10.1175/1525-7541(2003)004<0782:ERIFWR>2.0.CO;2.

Nicholas, C. A., and R. Larkin (1976), Raindrop-size distributions in a hilly region, *Meteorol. Mag.*, *105*, 361–381.

Norbiato, D., M. Borga, M. Sangati, and F. Zanon (2007), Regional frequency analysis of extreme precipitation in the eastern Italian Alps and the August 29, 2003 flash flood, *J. Hydrol.*, *345*, 149–166, doi:10.1016/j.jhydrol.2007.07.009.

Petersen, W. A., L. D. Carey, S. A. Rutledge, J. C. Knievel, N. J. Doesken, R. H. Johnson, T. B. McKee, T. Vonder Haar, and J. F. Weaver (1999), Mesoscale and radar observations of the Fort Collins flash flood of 28 July 1997, *Bull. Am. Meteorol. Soc.*, *80*(2), 191–216, doi:10.1175/1520-0477(1999)080<0191:MAROOT>2.0.CO;2.

Pope, G. L., P. D. Rigas, and C. F. Smith (1998), Statistical summaries of streamflow characteristics of drainage basins for selected streamflow-gaging stations in Arizona through water year 1996, *U.S. Geol. Surv. Water Resour. Invest. Rep., 98-4225*, 905 pp.

Pytlak, E., M. Goering, and A. Bennett (2005), Upper tropospheric troughs and their interaction with the North American Monsoon, paper presented at 85th Annual Meeting [CD-ROM], Am. Meteorol. Soc., San Diego, Calif.

Raghavan, S. (2003), *Radar Meteorology*, 549 pp., Kluwer Acad., Boston.

Roeske, R. H., M. E. Cooley, and B. N. Aldridge (1978), Floods of September 1970 in Arizona, Utah, Colorado, and New Mexico, *U.S. Geol. Surv. Water Supply Pap., 1052*, 135 pp.

Schaffner, M., and W. Reed (2005), Effects of Wildfire in the Mountainous Terrain of Southeast Arizona: Post-Burn Hydrologic Response of Nine Watersheds, *NOAA Natl. Weather Serv. Western Reg. Tech. Attachment 05-01*, 43 pp., NOAA Natl. Weather Serv., Silver Spring, Md.

Smith, J. A., M. L. Baeck, M. Steiner, and A. J. Miller (1996), Catastrophic rainfall from an upslope thunderstorm in the central Appalachians: The Rapidan storm of June 27, 1995, *Water Resour. Res.*, *32*, 3099–3113, doi:10.1029/96WR02107.

Stout, G. E., and E. A. Mueller (1968), Survey of relationships between rainfall rate and radar reflectivity in the measurement of precipitation, *J. Appl. Meteorol.*, *7*, 465–474, doi:10.1175/1520-0450(1968)007<0465:SORBRR>2.0.CO;2.

Webb, R. H., and J. L. Betancourt (1992), Climatic variability and flood frequency of the Santa Cruz River, Pima County, Arizona, *U.S. Geol. Surv. Water Supply Pap., 2379*, 40 pp.

Webb, R. H., C. S. Magirl, P. G. Griffiths, and D. E. Boyer (2008), Debris flows and floods in southeastern Arizona from extreme precipitation in July 2006: Magnitude, frequency, and sediment delivery, *U.S. Geol. Surv. Open File Rep., 2008-1274*, 95 pp.

Wohl, E. E., and P. A. Pearthree (1991), Debris flows as geomorphic agents in the Huachuca Mountains of southeastern Arizona, *Geomorphology*, *4*, 273–292, doi:10.1016/0169-555X(91)90010-8.

Zawadzki, I. (1973), Errors and fluctuations of rain gauge estimates of areal rainfall, *J. Hydrol.*, *18*, 243–255, doi:10.1016/0022-1694(73)90050-4.

Zehr, R. M., and V. A. Meyers (1984), Depth-area ratios in the semi-arid southwest United States, *Tech. Memo. NWS HYDRO-40*, 45 pp., NOAA Natl. Weather Serv., Silver Spring, Md.

P. G. Griffiths and R. H. Webb, U.S. Geological Survey, 520 N. Park Avenue, Tucson, AZ 85719, USA. (pggriffi@usgs.gov)

S. W. Lyon, Physical Geography and Quaternary Geology, Stockholm University, SE-106 91 Stockholm, Sweden.

C. S. Magirl, U.S. Geological Survey, 934 Broadway, Tacoma, WA 98402, USA.

E. Pytlak, NOAA/National Weather Service, 520 North Park Avenue, Tucson, AZ 85719, USA.

P. A. Troch, Hydrology and Water Resources, University of Arizona, Tucson, AZ 85719, USA.